Monthly Notices
of the
ROYAL ASTRONOMICAL SOCIETY

MNRAS **455,** 1246–1256 (2016) doi:10.1093/mnras/stv2388

Supervoids in the *WISE*–2MASS catalogue imprinting cold spots in the cosmic microwave background

F. Finelli,[1,2] J. García-Bellido,[3]★ A. Kovács,[4] F. Paci[5] and I. Szapudi[6]

[1]*INAF-IASF Bologna, Istituto di Astrofisica Spaziale e Fisica Cosmica di Bologna Istituto Nazionale di Astrofisica, via Gobetti 101, I-40129 Bologna, Italy*
[2]*INFN, Sezione di Bologna, Via Irnerio 46, I-40126 Bologna, Italy*
[3]*Instituto de Física Teórica IFT-UAM/CSIC, Universidad Autónoma de Madrid, Cantoblanco, E-28049 Madrid, Spain*
[4]*Institut de Física d'Altes Energies, Universitat Autónoma de Barcelona, E-08193 Bellaterra (Barcelona), Spain*
[5]*SISSA, Astrophysics Sector, Via Bonomea 265, I-34136 Trieste, Italy*
[6]*Institute for Astronomy, University of Hawaii, 2680 Woodlawn Drive, Honolulu, HI 96822, USA*

Accepted 2015 October 14. Received 2015 October 12; in original form 2014 May 7

ABSTRACT

The Cold Spot (CS) is a clear feature in the cosmic microwave background (CMB); it could be of primordial origin, or caused by a intervening structure along the line of sight. We identified a large projected underdensity in the recently constructed *WISE*–2MASS all-sky infrared galaxy catalogue aligned with the CS direction at $(l, b) \approx (209^\circ, -57^\circ)$. It has an angular size of tens of degrees, and shows a ∼20 per cent galaxy underdensity in the centre. Moreover, we find another large underdensity in the projected *WISE*–2MASS galaxy map at $(l, b) \approx (101^\circ, 46^\circ)$ (hereafter Draco supervoid), also aligned with a CMB decrement, although less significant than that of the CS direction. Motivated by these findings, we develop spherically symmetric Lemaitre–Tolman–Bondi (LTB) compensated void models to explain the observed CMB decrements with these two underdensities, or 'supervoids'. Within our perturbative treatment of the LTB voids, we find that the integrated Sachs–Wolfe and Riess–Sciama effects due to the Draco supervoid can account for the CMB decrement observed in the same direction. On the contrary, the extremely deep CMB decrement in the CS direction is more difficult to explain by the presence of the CS supervoid only. Nevertheless, the probability of a random alignment between the CS and the corresponding supervoid is disfavoured, and thus its contribution as a secondary anisotropy cannot be neglected. We comment on how the approximations used in this paper, in particular the assumption of spherical symmetry, could change quantitatively our conclusions and might provide a better explanation for the CMB CS.

Key words: surveys – cosmic background radiation – cosmology: observations – large-scale structure of Universe.

1 INTRODUCTION

The temperature anisotropies of the cosmic microwave background (CMB) provide the earliest image of the primordial density fluctuations generated during inflation. They evolve into the present distribution of dark matter traced by galaxies, possibly in a biased fashion. The cosmological information encoded in the spatial distribution of galaxies is revealed by several present and future programmes mapping the Universe in wide area surveys, such as Pan-STARRS (Kaiser, Burgett & Chambers 2010), DES,[1] DESI (DESI Collaboration 2013), LSST (LSST Science Collaboration 2009) and Euclid (Euclid Collaboration 2011, 2013).

While a homogeneous and flat Universe with a cosmological constant and dark matter – the ΛCDM model – agrees with most of the observations, several 'anomalies' remain puzzling on large angular scales in the CMB maps. Among these, a cold area in the direction $(l, b) = (209^\circ, -57^\circ)$, initially found as of approximatively 5° radius in the *Wilkinson Microwave Anisotropy Probe* (*WMAP*) temperature map by Vielva et al. (2004), has been characterized in the *Planck* 2013 temperature maps with great accuracy (Planck Collaboration XXIII 2013). The occurrence of a decrement in the CMB temperature pattern with similar size in Gaussian simulations has been evaluated to be below 1 per cent (Cruz et al. 2005). Although the statistical significance of the cold spot (CS) as an anomaly in the CMB pattern within the ΛCDM cosmology can be debated, it is important to pursue physical explanations beyond assuming it is a statistical fluke.

The CS in the CMB pattern could have been originated by a primordial fluctuation on the last scattering surface or by an

★ E-mail: juan.garciabellido@uam.es
[1] http://www.darkenergysurvey.org/

intervening phenomenon along the line of sight. Contamination from our galaxy or by the Sunyaev–Zeldovich effect from a cluster are quite unlikely (Cruz et al. 2006). If it were a primordial feature on the last scattering surface, the CS could be a signature of a non-perturbative effect during inflation (García-Bellido & Haugboelle 2008; Afshordi, Slosar & Wang 2011), or it might open a new exciting window on to the early Universe if caused by a cosmic texture generated during a phase transition at 10^{16} GeV (Cruz et al. 2008). Alternatively, the CS could be imprinted by an intervening supervoid along the line of sight (Inoue & Silk 2006, 2007; Inoue, Sakai & Tomita 2010; Inoue 2012). While voids fill approximately 30 per cent of the Universe at $z < 1$ (Colberg et al. 2005) a quantitative explanation seems to require a supervoid with radius $\gtrsim$200 Mpc^{-1}, a quite rare structure in a ΛCDM cosmology. Future data from CMB lensing (Das & Spergel 2008) and from 21-cm observations (Kovetz & Kamionkowski 2013) may help to further discriminate between the texture and the void hypotheses.

The supervoid hypothesis can be tested in galaxy surveys, and several investigations have been already carried out. An underdensity in the direction of the CMB CS has been claimed in NVSS (Rudnick, Brown & Williams 2007), but its statistical significance has been debated (Smith & Huterer 2010). Granett, Szapudi & Neyrinck (2010) imaged the CS region by the Canada–France–Hawaii Telescope (CFHT) ruling out the existence of a 100 Mpc supervoid with underdensity $\delta \simeq -0.3$ at $0.5 < z < 0.9$. Bremer et al. (2010) reached similar conclusions from a redshift survey using the VIMOS spectrograph on the VLT. In the relatively shallow 2MASS galaxy catalogue, Francis & Peacock (2010) found an underdensity in the galaxy field in the CS region. The structure they identified induces a $\Delta T = -7\mu$K depression in the CMB temperatures in the ΛCDM cosmology, that is not a satisfactory explanation for the CS anomaly.

In this paper and in Szapudi et al. (2015), a supervoid is indeed found in the direction of the CMB CS at a redshift compatible with previous constraints (Bremer et al. 2010; Granett et al. 2010). In this paper, we characterize the underdensity with the use of the recent galaxy catalogue *WISE*–2MASS (Kovács & Szapudi 2014) produced by joining the *Wide-Field Infrared Survey Explorer* (*WISE*; Wright et al. 2010) with the 2-Micron All-Sky Survey (2MASS; Skrutskie et al. 2006), whose median redshift is $z \sim 0.14$. (See Kovács et al. 2013 for the previous generation of catalogue based on *WISE* alone.) In Szapudi et al. (2015), a joint *WISE*–2MASS-Pan-STARRS1 catalogue constructed within a $50^\circ \times 50^\circ$ area centred on the CMB CS with photometric redshifts is used to best characterize the supervoid and determine also its deepest region at $z \sim 0.15$–0.25.

Motivated by this detection of a supervoid in the direction of the CMB CS we use an LTB model to jointly explain the underdensity in the *WISE*–2MASS galaxy survey and the decrement in the CMB temperature maps. Since a correspondence between supervoids and cold regions in the CMB temperature pattern could not be unique to the CS direction, we search for other large underdensities in the *WISE*–2MASS catalogue, extending Szapudi et al. (2015) who surveyed only the CS area. We find *another* underdensity located in the Northern Galactic hemisphere in the direction at ($l \approx 101^\circ$, $b \approx 46^\circ$) with an angular size similar to the one found in the direction of the CMB CS. While this projected underdensity is even deeper than the one found in the CS region, the shallow 2MASS galaxy density maps of $z_{\rm mean} = 0.07$ by Rassat, Starck & Dupé (2013) show a large underdensity in a similar location, therefore it may be closer to us and smaller in physical size. Hereafter, we refer to this underdensity as Draco supervoid. Since this underdensity is aligned with a moderate CMB temperature decrement as well, we apply our LTB model to jointly explain the galaxy and CMB pattern in this direction.

The paper is organized as follows. In Section 2, we briefly describe the *Planck* nominal mission and *WMAP* 9-yr temperature data which we use for our analysis, and also describe the *WISE*–2MASS data and the two largest underdensities found. In Section 3, we describe our basic LTB model for voids and the corresponding predictions for CMB temperature anisotropies, and apply our basic LTB model to the underdensities found in the *WISE*–2MASS catalogue. We draw our conclusions in Section 4.

2 DATA SETS

2.1 Cmb temperature maps

As CMB temperature maps we consider *WMAP* 9-yr and *Planck* data. To minimize astrophysical contamination, we use CMB foreground cleaned maps. For *WMAP*, we use the 9th year Internal Linear Combination (ILC) map at the HEALPIX (Gorski et al. 2005) resolution $N_{\rm side} = 1024$ publicly provided at http://lambda.gsfc.nasa.gov/. For *Planck* data, different CMB foreground cleaned maps are provided Planck Collaboration XII (2013), and we choose the Spectral Matching Independent Component Analysis (SMICA) (Cardoso et al. 2008) map at the HEALPIX (Gorski et al. 2005) resolution $N_{\rm side} = 2048$, publicly provided at http://pla.esac.esa.int/pla/aio/planckProducts.html.

2.2 *WISE*–2MASS galaxies

Kovács & Szapudi (2014) combined photometric information of the *WISE* and 2MASS infrared all-sky surveys to produce a clean galaxy sample for large-scale structure research. They apply Support Vector Machines (SVM) to classify objects using the multicolour *WISE*–2MASS data base. They calibrate their star–galaxy separator algorithm using Sloan Digital Sky Survey (SDSS; Abazajian et al. 2009) classification, and use the Galaxy and Mass Assembly (GAMA; Driver et al. 2011) spectroscopic survey for determining the redshift distribution of the *WISE*–2MASS galaxy sample.

Furthermore, Kovács & Szapudi (2014) pointed out that $W1_{\rm WISE} - J_{\rm 2MASS} \leq -1.7$ with a flux limit of $W1_{\rm WISE} \leq 15.2$ mag is a simple and effective star–galaxy separator, capable of producing results comparable to the multidimensional SVM classification. As a further refinement, another flux limit of $J_{\rm 2MASS} \leq 16.5$ mag is applied to have a fairly uniform all-sky data set that is deeper than 2MASS XSC (Jarrett et al. 2000) and cleaner the *WISE*. The final catalogue has an estimated ∼2 per cent stellar contamination among 2.4 million galaxies with $z_{\rm med} \approx 0.14$.

We construct a mask to exclude potentially contaminated regions near the Galactic plane using the dust emission map of Schlegel, Finkbeiner & Davis (1998). We mask out all pixels with $E(B-V) \geq 0.1$, and regions at galactic latitudes $|b| < 20^\circ$, leaving 21 200 deg^2 for our purposes. The resulting galaxy density map with the corresponding mask is shown in Fig. 1.

2.2.1 *CS region in* WISE–*2MASS*

We first study the CMB CS region on the sky as traced by *WISE*–2MASS galaxies in the ∼30 arcmin resolution 2D projection – `HEALPix` (Gorski et al. 2005) $N_{\rm side} = 128$ – therefore perform a complementary analysis to that of Szapudi et al. (2015) who measured galaxy densities in the line of sight in their *WISE*–2MASS-PS1

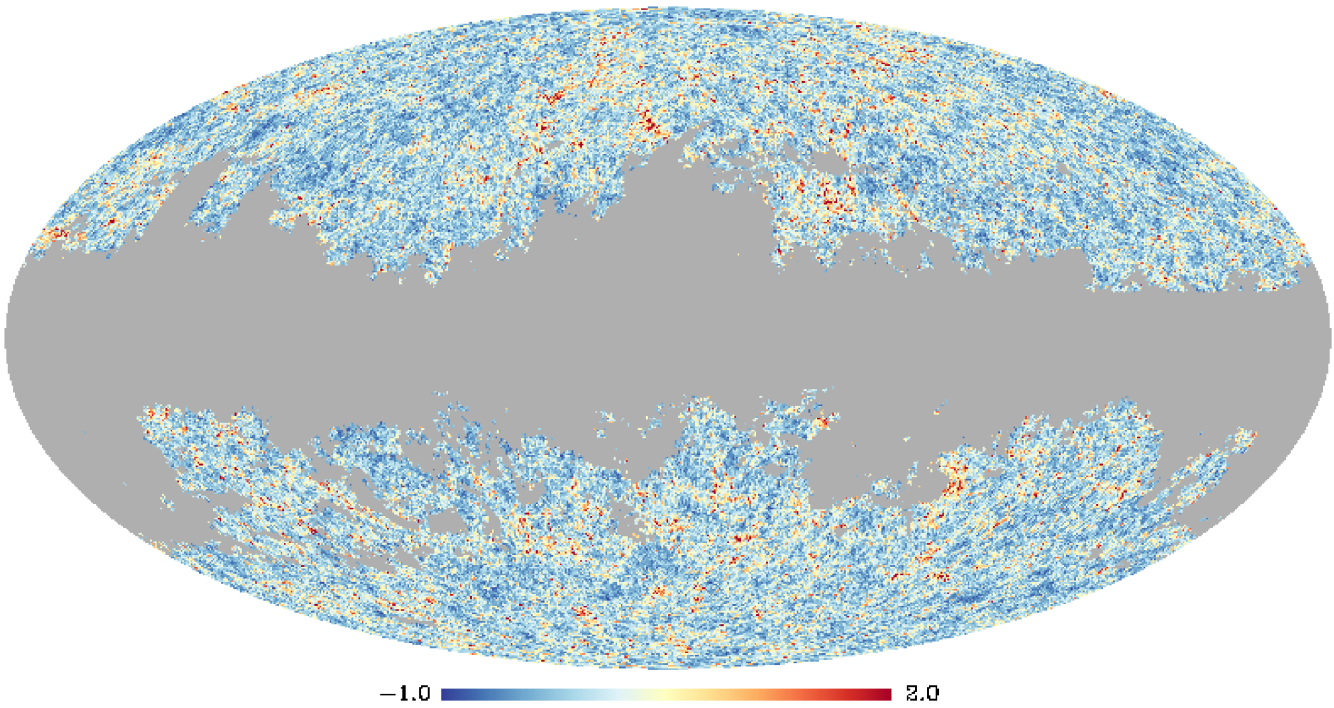

Figure 1. *WISE*–2MASS galaxy density map with the corresponding mask. We show the relative number-count deviations from the mean. Regions with values −1 correspond to empty regions, while values of 2 correspond to high-density regions.

photo-z data. Top panel of Fig. 2 shows a $60^\circ \times 60^\circ$ size patch of the galaxy catalogue, centred on the CS direction. At the centre of the CS, there is an approximately 20 per cent underdensity in galaxy counts, extending for a radius over 20°. We observed that the deepest part of this underdensity is slightly off-centre with respect to the centre of the CS estimated based on CMB data, but we only use this nominal centre in our analysis to minimize posteriori choices.

The image in the *WISE*–2MASS galaxy catalogue is compared to the same angular patch of the *WMAP* 9-year Internal Linear Combination (ILC) map (WMAP Collaboration 2013) and of the *Planck* SMICA map (Planck Collaboration XII 2013) in Fig. 2. An average 70 μK temperature decrement of approximatively 10° in size is clearly visible, corresponding to the CMB CS (Cruz et al. 2005).

2.2.2 *Further large voids in* WISE–*2MASS?*

We proceed with identifying underdensities in *WISE*–2MASS that are comparable to that of the CMB CS region. The galaxy density field was smoothed with a $\sigma = 20^\circ$ Gaussian kernel to filter out all underdensities smaller than the angular radius of the supervoid found at the CS. All pixels as 'cold' as the CS supervoid region have been selected. Our findings are summarized in Fig. 3. There is another large underdensity in the *WISE*–2MASS catalog that has similar angular size to the CS. Moreover, this underdensity is somewhat deeper in its centre, as shown in Fig. 2. We deem the centre of the void as the coldest pixel's location at $\ell \approx 101^\circ$, $b \approx 46^\circ$, and for simplicity we call it the Draco supervoid to distinguish it form the CS void. The $60^\circ \times 60^\circ$ size patch of the galaxy and the CMB field corresponding to the draco supervoid is shown in Fig. 4.

A 5° Gaussian smoothed version of the CS and the Draco void field is shown in Fig. 5.

3 THE BASIC ΛLTB VOID MODEL

We model an underdensity in *WISE*–2MASS as a compensated void profile within a ΛLTB model, (García-Bellido & Haugboelle 2008),

$$\mathrm{d}s^2 = -\mathrm{d}t^2 + \frac{A'(r,t)^2}{1-k(r)}\,\mathrm{d}r^2 + A(r,t)^2\,\mathrm{d}\Omega^2\,, \tag{1}$$

characterized by a spatial curvature profile given by

$$k(r) = k_0\, r^2 \exp\left[-\frac{r^2}{r_0^2}\right]. \tag{2}$$

See also Romano et al. (2014) for a recent use of a Gaussian profile for LTB models in another context. We approximate the novel ΛLTB model introduced above as a linear perturbation Φ in the synchronous gauge in a Friedman–Robertson–Walker (FRW) metric with $\Omega_\mathrm{M} + \Omega_\Lambda = 1$:

$$\Phi(\tau, r) = \Phi_0(r)\; {}_2F_1\left[1, \frac{1}{3}, \frac{11}{6}, -\frac{\Omega_\Lambda}{\Omega_\mathrm{M}} a^3\right], \tag{3}$$

$$\equiv \Phi_0 \exp\left[-\frac{r^2}{r_0^2}\right] F_1(u) \tag{4}$$

where $u = \frac{\Omega_\Lambda}{\Omega_\mathrm{M}} a^3$ and τ is the FRW conformal time:

$$\tau(a) = \frac{2\sqrt{a}}{H_0\sqrt{\Omega_\mathrm{M}}}\; {}_2F_1\left[\frac{1}{2}, \frac{1}{6}, \frac{7}{6}, -\frac{\Omega_\Lambda}{\Omega_\mathrm{M}} a^3\right] \equiv \frac{2\sqrt{a}}{H_0\sqrt{\Omega_\mathrm{M}}}\, F_2(u). \tag{5}$$

The scalar potential (4) gives rise to a 3D density profile for the void, via Poisson equation $\nabla^2\Phi = \frac{3}{2} H_0^2 \Omega_\mathrm{M}\, \delta/a$,

$$\delta(\tau, r) = -\delta_0\, g(\tau)\left(1 - \frac{2}{3}\frac{r^2}{r_0^2}\right) \exp\left[-\frac{r^2}{r_0^2}\right], \tag{6}$$

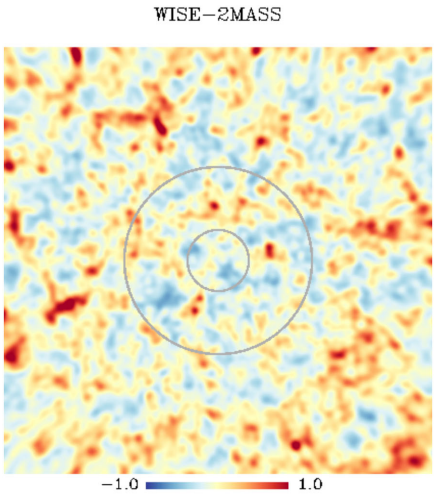

Figure 2. The *WISE*–2MASS (top), *WMAP*9 (middle), and *Planck* SMICA (bottom) field in the direction of the CS. Circles correspond to 5° and 15° radii. The top panel shows the same as in Fig. 1.

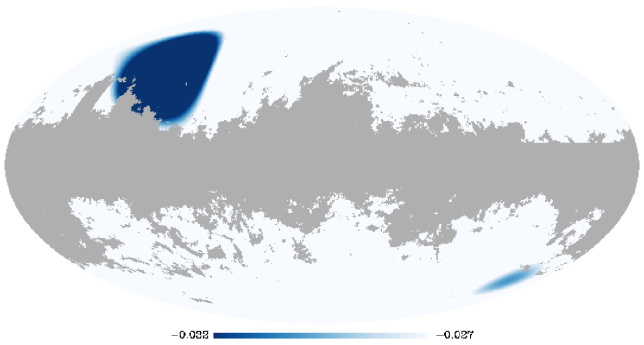

Figure 3. Applying a $\sigma = 20^\circ$ Gaussian smoothing to the *WISE*–2MASS galaxy map one finds two large underdensities on the full observable sky. One of them is the famous CS region, the other one is the Draco supervoid.

characterized by two parameters, the comoving width of the void, r_0,[2] and its depth today, δ_0. The following relation between Φ_0, k_0 and r_0 holds

$$\Phi_0 = \frac{-3k_0 r_0^2}{40} = \frac{\Omega_\mathrm{M}}{4}\frac{H_0^2\, r_0^2\, \delta_0}{F_1(-\Omega_\Lambda/\Omega_\mathrm{M})}\,. \tag{7}$$

We write the density contrast growth factor $g(a)$ as

$$g(a) \equiv \frac{\delta(a)}{\delta(1)} = \frac{a\, F_1(u)}{F_1(-\Omega_\Lambda/\Omega_\mathrm{M})}\,.$$

It is easy to check that the 3D density profile (6) gives rise to a *compensated void*,

$$\int_0^\infty \mathrm{d}r\, r^2\, \delta(r,\tau) = 0, \tag{8}$$

a property which will be useful later.

In order to compare with *WISE*–2MASS, we project the 3D density (6) on to the transverse plane, with the centre of the void at comoving distance y_0, see Fig. 6. The relation between r and θ is given by $r^2(y,\theta) = y^2 + y_0^2 - 2yy_0\,\cos\theta$,

$$\delta_\mathrm{2D}(\theta) = \int_0^\infty \delta\left(r(y,\theta)\right)\, y^2\phi(y)\mathrm{d}y\,, \tag{9}$$

with $y = r(z)$ and $y_0 = r(z_0)$ are the comoving distances to the void, and $\phi(y)$ is the *WISE*–2MASS window function.

From the metric perturbation (4), we now compute the linear Integrated Sachs–Wolfe (ISW henceforth) (Sachs & Wolfe 1967; Kofman & Starobinsky 1985) and the non-linear Rees–Sciama (RS henceforth) (Rees & Sciama 1968) effect on the CMB temperature anisotropies. For a large compensated void with a profile as in equation (6), the linear ISW effect is given by

$$\begin{aligned}\frac{\delta T}{T}^{\mathrm{ISW}}(\theta) &= 2\int_{\tau_0}^{\tau_E}\mathrm{d}\tau\,\dot\Phi(\tau,r)\\ &= -\frac{12}{11}\frac{\Omega_\Lambda}{\Omega_\mathrm{M}}\int_0^1 \mathrm{d}a\, a^2\Phi_0(r)\,{}_2F_1\left[2,\,\frac{4}{3},\,\frac{17}{6},\,\frac{-\Omega_\Lambda a^3}{\Omega_\mathrm{M}}\right]\\ &\equiv -\frac{12}{11}\frac{\Omega_\Lambda}{\Omega_\mathrm{M}}\int_0^1 \mathrm{d}a\, a^2\Phi_0(r(z,\theta))\, F_4(u)\,,\end{aligned} \tag{10}$$

[2] In the first version of this manuscript, we followed Masina & Notari (2009) and considered a large difference between the FRW and the ΛLTB radii. This difference was due to an incorrect matching of the ΛLTB void to an Einstein–de Sitter model with $\Omega_\mathrm{M} = 1$, which was performed by Biswas & Notari (2008) for a different physical problem. The FRW and ΛCDM radii are now approximatively the same as in Zibin (2014) and Nadathur et al. (2014).

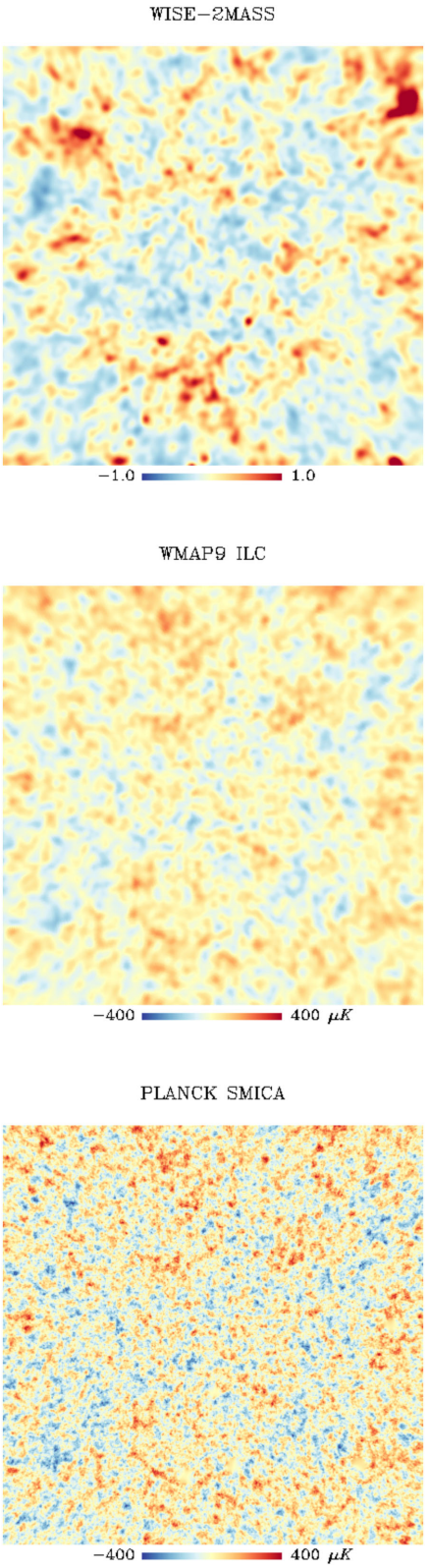

Figure 4. The *WISE*–2MASS (top), *WMAP*9 (middle), and *Planck* SMICA (bottom) field in the direction of the Draco void. The top panel shows the same as in Fig. 1.

where

$$r^2(z,\theta) = r^2(z) + r^2(z_0) - 2\,r(z)r(z_0)\cos\theta,$$

and we integrate over z. Note that the comoving distance is given by $r(z) = \tau_0 - \tau(z)$, see equation (5).

For the Gaussian profile in equation (4) we find, in the small angle approximation, with $r(z_0) > r_0$,

$$\frac{\delta T}{T}^{\rm ISW}(\theta) \simeq -\frac{3\sqrt{\pi}}{22}\frac{H(z_0)\,\Omega_\Lambda\,F_4(-\Omega_\Lambda/\Omega_{\rm M}(1+z_0)^3)}{H_0\,(1+z_0)^4\,F_1(-\Omega_\Lambda/\Omega_{\rm M})}\times \left(1+{\rm erf}\left[\frac{z_0}{H(z_0)r_0}\right]\right)\delta_0\,(H_0 r_0)^3\exp\left[-\frac{r^2(z_0)}{r_0^2}\theta^2\right], \tag{11}$$

which also gives a Gaussian profile for the ISW effect.

Following Tomita (2005) and Tomita & Inoue (2008), we compute the RS effect on the CMB temperature anisotropies as

$$\frac{\delta T}{T}^{\rm RS}(\theta) = \int_0^{z_{\rm LS}} {\rm d}z\left[4\zeta_1'(z)\frac{r^2(z,\theta)}{r_0^2} + 9\zeta_2'(z)\right] \times \frac{100}{9}\frac{\Phi_0^2}{r_0^2}\exp\left[-2\frac{r^2(z,\theta)}{r_0^2}\right], \tag{12}$$

where primes denote differentiation w.r.t. redshift and

$$\zeta_1(z) = \frac{3\,\tau^2}{200}\frac{F_1^2(u)}{F_2^2(u)}, \tag{13}$$

$$\zeta_2(z) = \frac{-\tau^2}{210}\frac{1}{F_2^2(u)}\left[\frac{7}{5}\left(\frac{5}{6}F_1(u) + \frac{1}{6}F_3^2(u)\right) - \frac{2}{5}\sqrt{1+u}\left(F_1(u)F_3(u) - \frac{5}{12}G(u)\right)\right], \tag{14}$$

$$G(u) = \frac{1}{3}u^{-7/6}\int\frac{{\rm d}u\,u^{1/6}}{\sqrt{1+u}}\left[F_3^2(u) - F_1(u)\right]. \tag{15}$$

Doing the integral in z, in the small angle approximation,

$$\frac{\delta T}{T}^{\rm RS}(\theta) \simeq -\frac{100}{9}\sqrt{\frac{\pi}{8}}\left(4\zeta_1'(z_0)\frac{r^2(z_0)}{r_0^2}\,\theta^2 + 9\zeta_2'(z_0)\right)H_0^2 \times\left(1+{\rm erf}\left[\frac{\sqrt{2}\,z_0}{H(z_0)r_0}\right]\right)\frac{\Phi_0^2(r_0,\delta_0)}{H_0\,r_0}\exp\left[-2\frac{r^2(z_0)}{r_0^2}\,\theta^2\right]. \tag{16}$$

The ISW and RS effects are shown in Fig. 7. The RS effect is quadratic in δ_0 and cubic in r_0, but smaller than the ISW effect in a ΛCDM cosmology.[3]

3.1 Predictions for the Draco supervoid

We construct a χ^2 statistics corresponding to the fits for the projected LTB model in the *WISE*–2MASS catalogue (denoted by the pedix LSS) and the corresponding effect on the *Planck* temperature anisotropy pattern (denoted by the pedix CMB). As primary parameters, we chose $\{\theta_i\} = \{\delta_0, r_0, z_0\}$, giving the following:

$$\chi^2_{\rm LSS} = \sum_{ij}\left(\delta_{\rm 2D}(\theta_i) - \delta_i^{\rm LSS}\right)D_{ij}^{-1}\left(\delta_{\rm 2D}(\theta_j) - \delta_j^{\rm LSS}\right), \tag{17}$$

[3] In the first version of this manuscript, we evaluate a much larger RS effect, mainly due to a wrong mismatch between the LTB and FRW radius, following Masina & Notari (2009). Our RS (and ISW) calculation for the novel profile in equation (2) now agrees with Zibin (2014) and, Nadathur et al. (2014).

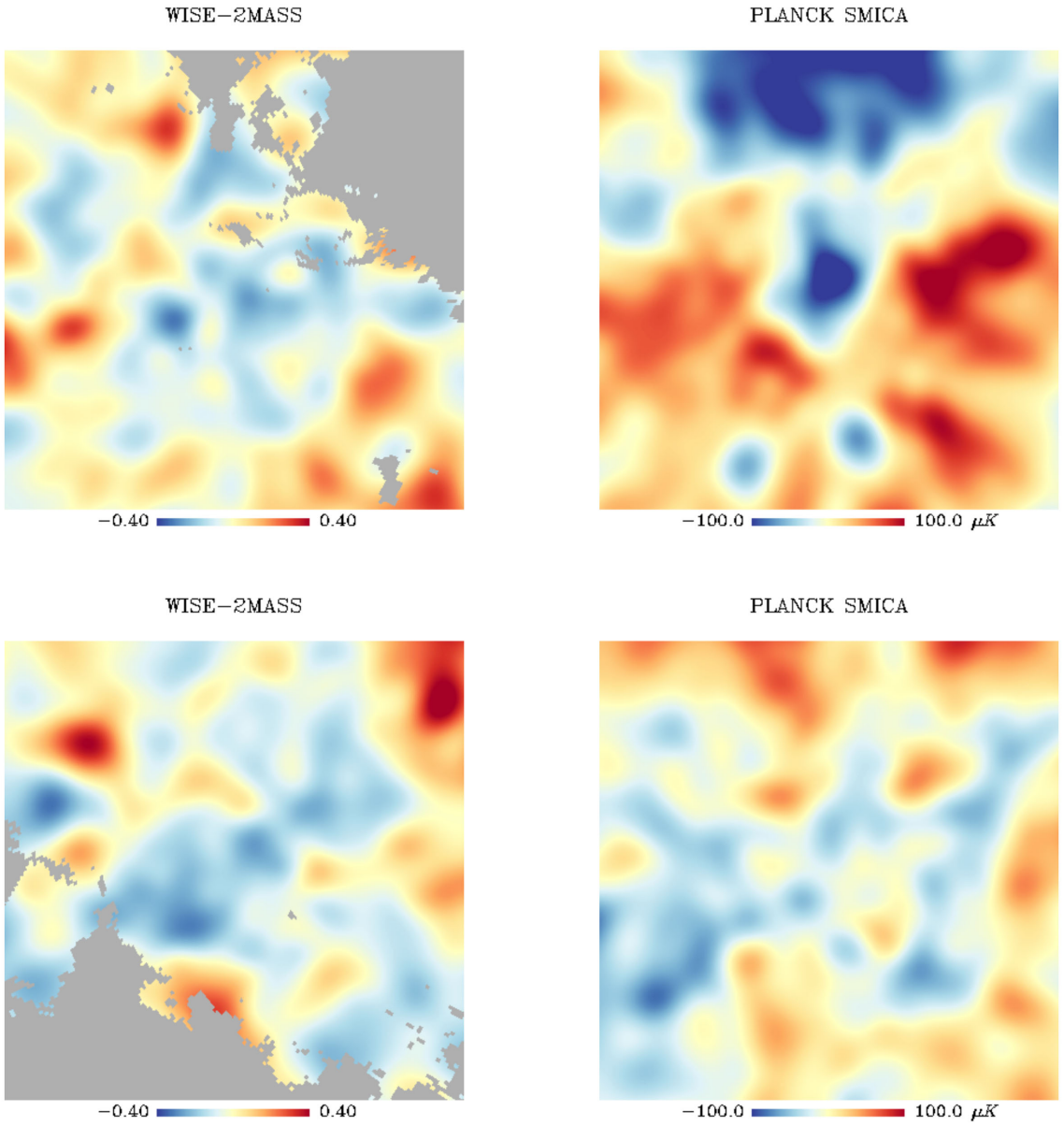

Figure 5. Top panels: the 5° Gaussian smoothed *WISE*–2MASS (left), and *Planck* SMICA (right) field in the direction of the CS. Bottom panels: same data in the direction of the Draco supervoid. The grey area in the *WISE*–2MASS panels shows the Galactic region we mask out for our analysis. The left-hand panels show the same as in Fig. 1.

$$\chi^2_{\rm CMB} = \sum_{ij} \left(\delta T(\theta_i) - \delta T_i^{\rm CMB}\right) C_{ij}^{-1} \left(\delta T(\theta_j) - \delta T_j^{\rm CMB}\right). \qquad (18)$$

The term in equation (17) corresponds to the χ^2 of the projected LTB void profile (9) with respect to the observed *WISE*–2MASS galaxy distribution, using the highly correlated covariance matrix D_{ij} of concentric rings in *WISE*–2MASS. We estimated the covariances by generating 10,000 Gaussian realizations of the projected *WISE*–2MASS map with `Healpix synfast`. The simulations were created assuming *Planck* cosmology, and the redshift distribution of the *WISE*–2MASS sources.

The term in equation (18) is the χ^2 of the CMB profile compared to the covariance matrix of rings in the CMB is also highly correlated. The covariance matrix was determined from 10,000 Gaussian CMB realizations. Note the covariance of the CMB at the angular scales considered is dominated by cosmic variance, thus neglecting the cross-correlation with LSS is a good approximation.

In order to match the data to the LTB prediction, we followed Kovács et al. (2013) and Szapudi et al. (2015), and estimated the bias of the galaxy catalogue using `SpICE` (Szapudi et al. 2001) and python CosmoPy[4] package, finding $b = 1.41 \pm 0.07$. The depression in galaxy counts, therefore, corresponds to a $\delta_{\rm 2D} = \delta_{\rm 2D,g}/b$ underdensity in matter, assuming linear bias relation.

According to equation (17), the best-fitting marginalized parameters to *WISE*–2MASS data alone is $\delta_0 = 0.40 \pm 0.20$, $r_0 = 210 \pm 70$ Mpc h^{-1} at 68 per cent CL. While from equation (18), the best

[4] http://www.ifa.hawaii.edu/cosmopy/

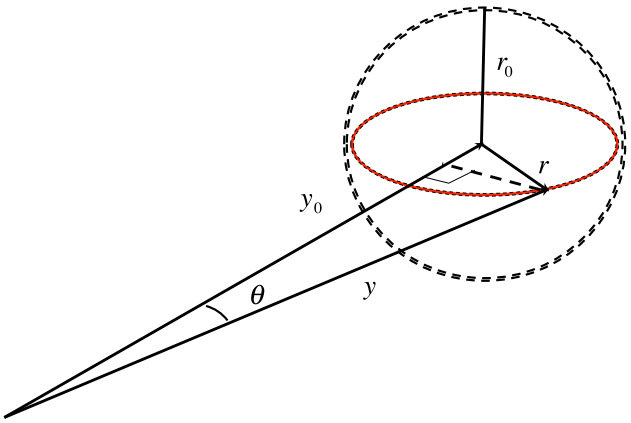

Figure 6. The corresponding geometry of the 2D projection of the LTB void for the *WISE*–2MASS projected galaxy contrast. The observer is at a comoving distance y_0 from the centre of the void.

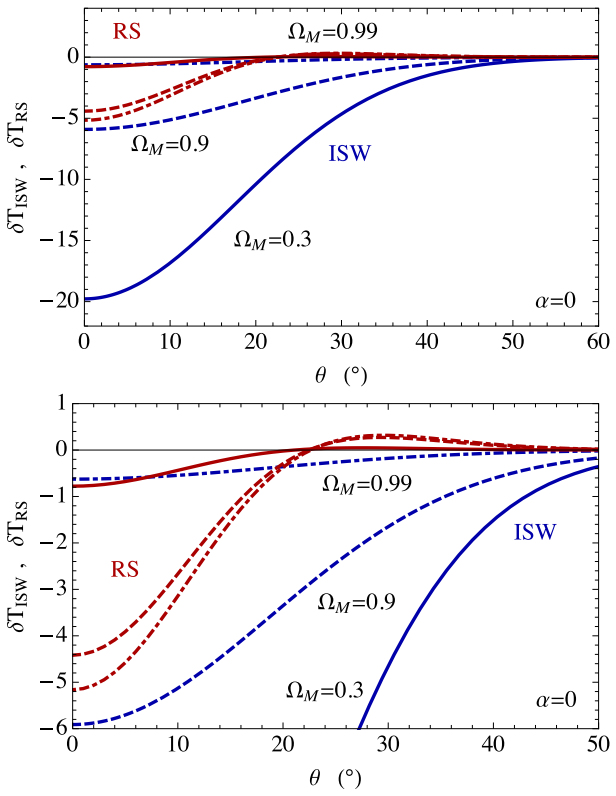

Figure 7. In the top panel the ISW (blue) and RS (red) effect for LTB voids with the profile introduced in equation (2) within our perturbative treatment are displayed for different values of $\Omega_M = 0.3$ (solid), $\Omega_M = 0.9$ (dashed), $\Omega_M = 0.99$ (dot–dashed). In the bottom panel, we zoom on the RS effect to show how its angular dependence differs from the one of the ISW term. The parameters of the void are $r_0 = 195$ Mpc/h, $\delta_0 = 0.25$, $z_0 = 0.155$.

fit to *Planck* data alone is $\delta_0 = 0.23 \pm 0.40$, $r_0 = 290 \pm 90$ Mpc h^{-1} at 68 per cent CL.[5]

[5] The χ^2 statistic for the radial density profile measurement *compared to a null value* in each bin, and found $\chi^2 = 65.22$ for 24 degrees of freedom, i.e. $p = 10^{-5}$ as a simple estimate of the extremeness of the Draco supervoid in *WISE*–2MASS.

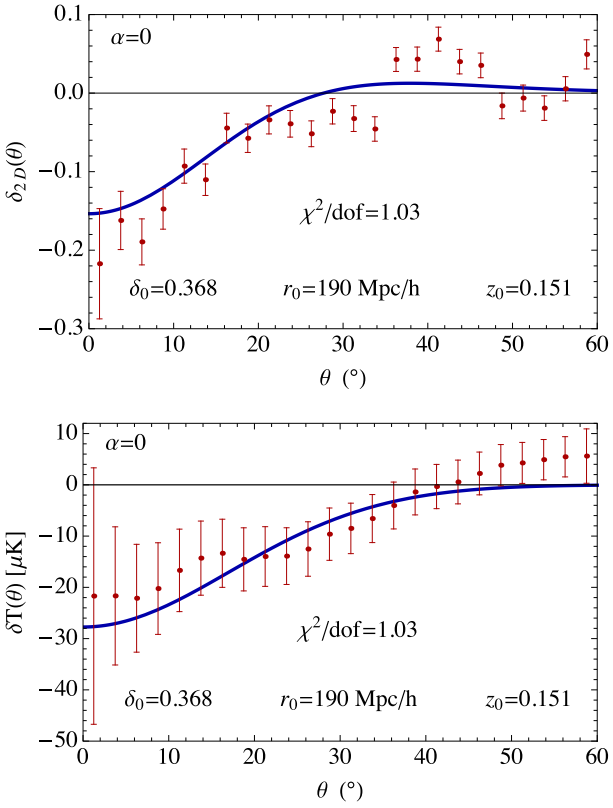

Figure 8. The density profile from *WISE*–2MASS catalogue compared with the best-fitting theoretical model for the underdensity (9) from a combined analysis (top panel). The temperature profile from *Planck* SMICA map (bottom panel) is compared with the predicted CMB signal. The blue lines are the theoretical profiles for rings and in red are the measurements.

We now estimate a simultaneous fit of *WISE*–2MASS and *Planck* data by:

$$\chi^2_{\rm tot}(\delta_0, r_0, z_0) = \chi^2_{\rm LSS} + \chi^2_{\rm CMB}. \quad (19)$$

Simultaneous minimization yields the best-fitting parameters, which we quote here with marginalized 1σ errors,

$$\delta_0 = 0.37^{+0.22}_{-0.12}\ (1\sigma), \quad (20)$$

$$r_0({\rm Mpc}\,h^{-1}) = 190^{+39}_{-27}\ (1\sigma), \quad (21)$$

$$z_0 = 0.15^{+0.04}_{-0.05}\ (1\sigma), \quad (22)$$

which are in good agreement with the best fits obtained separately from *WISE*–2MASS and *Planck*, and with the *WISE*–2MASS window function. The 1σ and 2σ contours of the size and depth parameters of the LTB void are shown in Fig. 9.

Note that the only constraint on the redshift of the void centre relies on the matching with the CMB profile in the location of the supervoid, and assuming a particular LTB void model. The approximate central redshift of $0.10 < z < 0.20$ is just compatible with our prior knowledge that the void might be located relatively close to us (Rassat et al. 2013). This slight tension indicates that in reality the void might be smaller in physical size and its cooling effect on the CMB is less significant assuming the same LTB model.

For later comparison, we calculate the averaged underdensity within the best-fitting radius $r_0 = 190\,h^{-1}$Mpc. The 3D

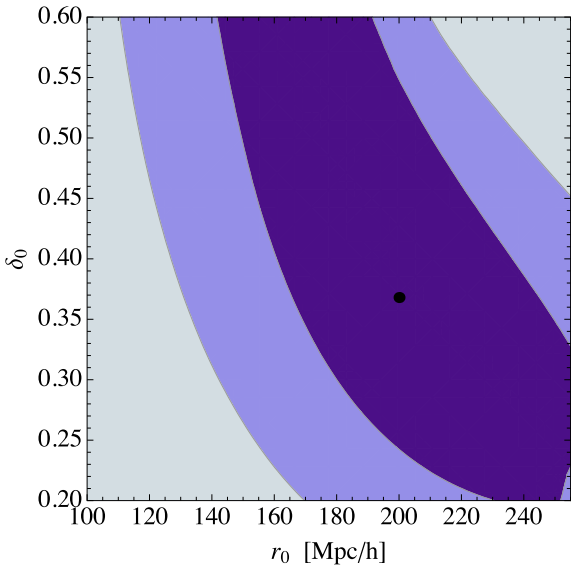

Figure 9. The 1σ and 2σ contours of the size and depth parameters of the LTB void (6), after marginalization over the redshift of the centre of the void with the *WISE*–2MASS window function.

top-hat-averaged density from the LTB profile, see equation (6), is $\bar{\delta} = 3/r_0^3 \int_0^{r_0} r^2 \mathrm{d}r\, \delta(r) = -\delta_0/e$. This finally gives the average void depth $\bar{\delta} = -0.14 \pm 0.03$.

In the ΛCDM model, the expected number of supervoids as extreme as the Draco supervoid at $z < 0.5$ is roughly $N \sim 10$ according to the estimations of Nadathur et al. (2014) in their Fig. 5. However, for a more realistic modelling of the actual survey volume filled by the *WISE*–2MASS catalogue, we need to take into account a masking factor $f_{\rm sky} = 0.53$, and the fact that the redshift distribution of the *WISE*–2MASS catalogue prevents reliable void identification at $z \geq 0.25$. The latter effectively results in a *WISE*–2MASS comoving survey volume that is only ∼15 per cent of the volume considered in Nadathur et al. (2014). Including these factors, we estimate a probability of $p \approx 0.8$ for finding a void at least as extreme as the Draco void in the *WISE*–2MASS survey volume.

3.2 Modelling of the CS

We now analyse an LTB description for the supervoid found in the CS direction. By using the results in Section 4 we obtain the marginalized over redshift best fit to *WISE*–2MASS data with reduced $\chi^2 = 0.85$ and $\delta_0 = 0.29 \pm 0.19$, $r_0(\mathrm{Mpc}\,h^{-1}) = 198 \pm 90$ at 68 per cent CL.[6] As best fit to *Planck* data we obtain a reduced $\chi^2 = 1.2$ and $r_0(\mathrm{Mpc}\,h^{-1}) = 136 \pm 50$, at 68 per cent CL, with no constraint on δ_0.

As is clear from the discussion above, the angular profile of the temperature decrement in the CS cannot be properly fit by the ISW+RS effect described in Section 3. The CMB imprint computed in Section 3 does not exhibit any ridge about 15° which instead characterizes the CS (Zhang & Huterer 2010 noticed this structure as an outer ring).

[6] The χ^2 statistic for the radial density profile measurement *compared to the null value in each bin* is 43.94 for 24 degrees of freedom, i.e. $p = 0.007$.

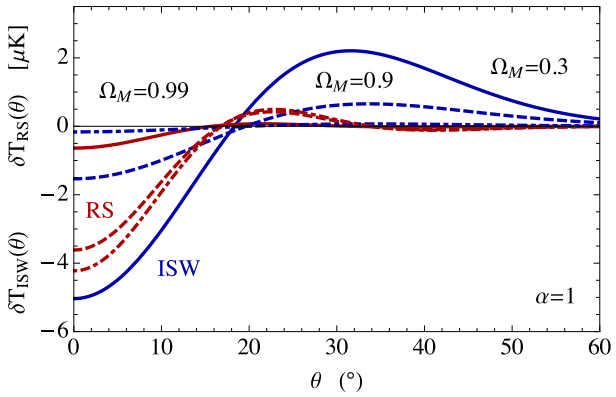

Figure 10. In the top panel the ISW (blue) and RS (red) effect for LTB voids with the profile introduced in equation (23) within our perturbative treatment are displayed for different values of $\Omega_M = 0.3$ (solid), $\Omega_M = 0.9$ (dashed), $\Omega_M = 0.99$ (dot–dashed). Note how for $\alpha = 1$ the angular profiles of the ISW and RS effects still differ, but now the ISW term exhibits a profile similar to a compensated one. The parameters of the void are $r_0 = 195$ Mpc/h, $\delta_0 = 0.25$, $z_0 = 0.155$.

We therefore modify the basic LTB profile by introducing a new parameter α,

$$\Phi_0(r) = \Phi_0 \left(1 - \alpha \frac{r^2}{r_0^2}\right) \exp\left[-\frac{r^2}{r_0^2}\right] \tag{23}$$

which corresponds to a density contrast:

$$\delta(\tau, r) = -\delta_0\, g(\tau) \left(1 - \frac{2+7\alpha}{3+3\alpha}\frac{r^2}{r_0^2} + \frac{2\alpha}{3+3\alpha}\frac{r^4}{r_0^4}\right) e^{-r^2/r_0^2}, \tag{24}$$

again giving rise to a *compensated void* (8), for all α. With these modifications, the ISW and RS angular profiles, for $0 < \alpha < 2$, are given by

$$\begin{aligned}\frac{\delta T}{T}^{\rm ISW}(\theta) \simeq & -\frac{3\sqrt{\pi}}{22} \frac{H(z_0)\,\Omega_\Lambda\, F_4(-\Omega_\Lambda/\Omega_{\rm M}(1+z_0)^3)}{(1+\alpha)H_0(1+z_0)^4\, F_1(-\Omega_\Lambda/\Omega_{\rm M})} \\ & \times \left(\frac{2-\alpha}{2} - \alpha\frac{r^2(z_0)}{r_0^2}\theta^2\right)\left(1 + \mathrm{erf}\left[\frac{z_0}{H(z_0)r_0}\right]\right) \\ & \times \delta_0\,(H_0 r_0)^3 \exp\left[-\frac{r^2(z_0)}{r_0^2}\theta^2\right],\end{aligned} \tag{25}$$

which now has a node and a positive maximum, and

$$\begin{aligned}\frac{\delta T}{T}^{\rm RS}(\theta) \simeq & -\frac{100}{9}\sqrt{\frac{\pi}{8}}\left[9\zeta_2'(z_0)\left(1 + \frac{\alpha}{2} + \frac{7}{16}\alpha^2\right)\right. \\ & + \left(4\zeta_1'(z_0)\left(1+\frac{\alpha}{2}\right) - 9\zeta_2'(z_0)\left(2\alpha + \frac{\alpha^2}{2}\right)\right)\frac{r^2(z_0)}{r_0^2}\theta^2 \\ & \left. + \left(9\zeta_2'(z_0)\,\alpha^2 - 4\zeta_1'(z_0)\,\alpha\right)\frac{r^4(z_0)}{r_0^4}\theta^4\right] H_0^2 \\ & \times \left(1 + \mathrm{erf}\left[\frac{\sqrt{2}\,z_0}{H(z_0)r_0}\right]\right)\frac{\Phi_0^2(r_0,\delta_0)}{H_0\, r_0} \exp\left[-2\frac{r^2(z_0)}{r_0^2}\theta^2\right].\end{aligned} \tag{26}$$

These two effects are shown in Fig. 10. Note how this new compensated void model leads to a completely different angular profile for the ISW term, reminiscent of a compensated structure in the CMB as well, although with a smaller amplitude with respect to $\alpha = 0$.

We choose from now on the parameter $\alpha = 1$. We then obtain a best fit to *WISE*–2MASS data with reduced $\chi^2 = 0.85$ (for 24 d.o.f.)

and $\delta_0 = 0.27 \pm 0.25$, $r_0(\mathrm{Mpc}\,h^{-1}) = 270 \pm 90$ at 68 per cent CL. By fitting to *Planck* data alone we obtain a similar radius, $r_0(\mathrm{Mpc}\,h^{-1}) = 254 \pm 50$ at 68 per cent CL, with a large underdensity, $\delta_0 > 0.6$ at 95 per cent CL, which is clearly too high for the ΛCDM model.

Our ΛLTB models for the *WISE*–2MASS underdensity and the CMB decrement in the direction of the CS are not as satisfactory as for the analogous alignment we have found in the direction of the Draco supervoid. Although we have introduced a second novel compensated LTB profile, which leads to an ISW plus RS angular profile reminiscent of the CMB decrement in the direction of the CS, we cannot find an amplitude which fits well *WISE*–2MASS and *Planck* simultaneously for $\alpha = 1$.

Given the current status of the *WISE*–2MASS observations, we cannot exclude that other values of α or other profiles could provide a better fit. Another issues are the approximations used in this paper, as the perturbative treatment in a flat FRW metric, the assumption of ΛCDM, or spherical symmetry. It is conceivable that the structure in the direction of the CS might not be well approximated by a spherical object and might be possibly elongated along the line of sight: in such a case the angular profile in the *WISE*–2MASS data would be smaller than the effective distance which enters in the CMB decrement. Although this calculation goes beyond the scope of the current paper, this different geometry for the underdensity would help in reconciling the amplitude of the CMB decrement with the underdensity seen in *WISE*–2MASS.

In fact, if we consider together two adjacent voids along the same line of sight, at two different redshifts, it is possible to find a reasonable minimum χ^2, at the expense of an unrealistic depth (i.e. high density contrast) for the furthest void, although with reasonable widths in both, see Fig. 11. The common reduced $\chi^2 = 0.96$ for the first void at $z_0 = 0.2$ with a width $r_0 = 220$ Mpc h^{-1} and depth $\delta_0 = 0.25$, and for the second void at $z_0 = 0.5$ with a width $r_0 = 350$ Mpc h^{-1} and depth $\delta_0 = 0.5$ with reduced $\chi^2 = 17.4/24$ d.o.f. for *WISE*–2MASS and $\chi^2 = 12.5/10$ d.o.f. for *Planck*.

For estimations of the cosmic rareness of the CS void, we rely on the (presumably more accurate) best-fitting void parameters obtained with photo-z mapping by the companion paper Szapudi et al. (2015) ($\delta_{2D} = 0.14$, $\delta_0 = 0.38$, $r_0 = 220$ Mpc h^{-1}). The probability of detecting supervoids at least as extreme as the CS supervoid at $z < 0.5$ is roughly $p \sim 0.1$ according to the estimations of Nadathur et al. (2014). Including the $f_{\mathrm{sky}} = 0.53$ and $V_{z<0.25}/V_{z<0.5} \approx 0.15$ factors, the estimated probability is $p \sim 0.01$ for finding a void at least as extreme as the CS void in the *WISE*–2MASS survey volume. Thus the CS void represents a rare fluctuation in ΛCDM, and its occurrence is less likely than that of the Draco supervoid. Note that the large errors on δ_0 and r_0 can result in drastic changes in the expected void probability and ISW–RS signal of such voids (Nadathur et al. 2014). We, therefore, refer to these probabilities as crude estimations of cosmic rareness.

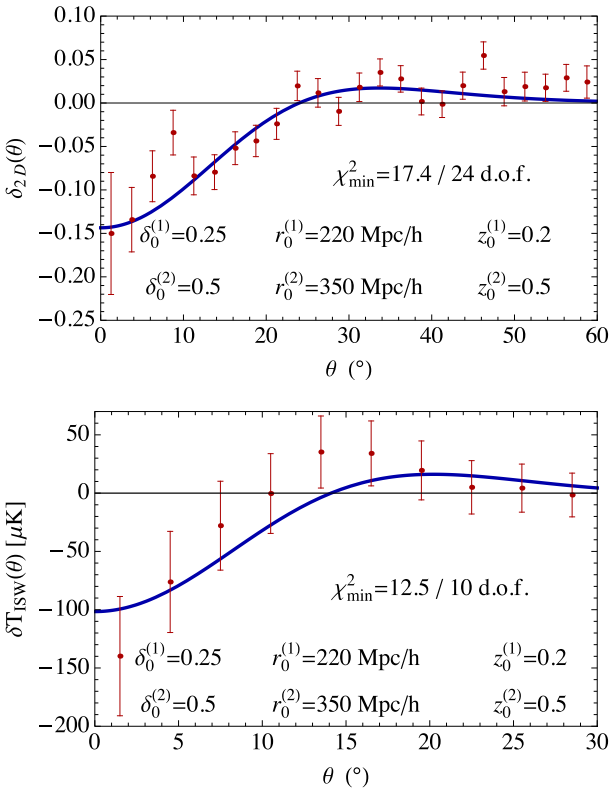

Figure 11. The density profile from *WISE*–2MASS catalogue compared with the theoretical model for the underdensity (9) (top panel). The temperature profile from *Planck* SMICA map (bottom panel) is compared with the predicted CMB signal. The blue lines are the theoretical profiles for rings and in red are the measurements. The model considers two adjacent spherical voids along the same line of sight with different sizes and depths.

4 DISCUSSION AND CONCLUSIONS

We have found two large underdensities in the *WISE*–2MASS catalogue (Kovács & Szapudi 2015) smoothed on 20° scales. The Draco supervoid is located at $(l, b) \approx (101°, 46°)$ and it corresponds to a gentle decrement in the CMB observed by both *WMAP* and *Planck*, and it is well explained by the ISW and RS effects. The other supervoid is in the well known direction of the CMB CS, and its explanation in terms of ISW and RS effect is less satisfactory. Nevertheless, observationally, we found that the two most prominent supervoids identified in a full sky catalog coincide with cold areas of the CMB.

A related project Szapudi et al. (2015) used the same *WISE*–2MASS data set supplemented with PS1 photometric redshifts and the data by Granett et al. (2010) for a direct tomographic imaging of the CS region. They found a supervoid at $z = 0.22 \pm 0.03$ with radius $r_0 = 220 \pm 50\,h^{-1}$Mpc and depth of $\delta = -0.14 \pm 0.04$.

Motivated by these findings, we developed novel spherically symmetric ΛLTB compensated void models to explain the CMB decrements observed in the direction of the two largest underdensities (supervoids) of the *WISE*–2MASS catalog. We compute perturbatively the projected angular density profile, and the ISW and RS angular profiles following the second order treatment presented in Tomita (2005) and Tomita & Inoue (2008).

Within our perturbative treatment of the simplest family of LTB voids introduced here with a Gaussian profile for the curvature, we find that the Integrated SW and RS effects due to the Draco supervoid found in the *WISE*–2MASS catalogue can explain well the CMB decrement observed in the same direction. By considering the combined fit with *WISE*–2MASS catalogue and *Planck* we obtain $\delta_0 = 0.37^{+0.22}_{-0.12}$, $r_0(\mathrm{Mpc}\,h^{-1}) = 190^{+39}_{-27}$, $z_0 = 0.15^{+0.04}_{-0.05}$ at 1σ as a best fit. The estimated redshift of the underdensity is in good agreement with the *WISE*–2MASS window function, but 2MASS-only observations of this underdense region by Rassat et al. (2013) indicate that the Draco void might be located closer to us, and therefore slightly smaller in physical size.

The explanation of the large decrement for the CS in terms of the ISW and RS effects is known to be difficult (Inoue & Silk 2006, 2007). The CMB angular profile of the CS, studied here at larger angular distances than those commonly considered ($\sim 10^\circ$), constitute also a puzzle with respect to the standard angular profiles previously studied (Inoue & Silk 2006, 2007) and those obtained here with the perturbative treatment of the simplest class of LTB voids. By introducing a further generalization of the LTB voids, which allows a more radical compensation, we indeed find an angular profile which better mimics what is observed in the CS, but with a much smaller amplitude for the underdensity found in the redshift range of the *WISE*–2MASS catalogue.

Given the status of the LSS observations and the assumptions used in this paper, more precise observations and further theoretical developments are needed before the CMB CS will be satisfactorily explained. On the observational ground, the 21 200 deg^2 photometric redshift catalog of *WISE*–2MASS galaxies matched with SuperCOSMOS data (Kovács et al., in preparation) will provide an enhanced tool for examining these structures and for identifying more superstructures in the low-z Universe.

Concerning the assumption of ΛCDM, there is some debate about the effects on the CMB being stronger than the simple predictions of the linear ISW model in a ΛCDM cosmology (e.g. Granett, Szapudi & Neyrinck 2008, 2010a; Papai & Szapudi 2010; Cai et al. 2014). We also mention how the assumption of spherical symmetry or the use of perturbation theory or the absence of cross-correlation between the SW and ISW terms in our calculation could be important quantitative aspects, which go beyond the scope of the present project.

Despite the assumptions and caveats mentioned above, let us finally note that this work, and the related project Szapudi et al. (2015), significantly increased the probability of a physical explanation of the CS instead of a statistical fluke. Given the rareness of the supervoid found in the CS direction, estimated here at about a 3σ deviation, we could ask for the probability of a random alignment of such a supervoid in the *WISE*–2MASS with a rare fluctuation in the CMB as the CS. Even considering the CS only as a 2σ fluctuation, the hypothesis of this alignment as a statistical fluke is quite low. We presented a quasi-linear ISW term with a angular profile similar to the CS and an amplitude larger than 20 μK obtained within spherical symmetry. Thus a fairly typical cold primordial fluctuation enhancing the ISW effect from the CS void on the CMB sky could provide a plausible explanation.

ACKNOWLEDGEMENTS

FF and JGB wish to thank the bilateral agreement INFN-CICYT and in particular, the director of the Bologna INFN section Dr G. Bruni for partially supporting this project. FF acknowledges the support by ASI through ASI/INAF Agreement I/072/09/0 for the *Planck* LFI Activity of Phase E2 and by MIUR through PRIN 2009 grant no. 2009XZ54H2. JGB acknowledges financial support from the Madrid Regional Government (CAM) under the programme HEPHACOS S2009/ESP-1473-02, from the Spanish MICINN grants AYA2009-13936-C06-06, FPA2012-39684-C03-02 and Consolider-Ingenio 2010 PAU (CSD2007-00060), and from the MINECO Centro de Excelencia Severo Ochoa Programme, grant SEV-2012-0249. In addition, AK takes immense pleasure in thanking the support provided by the Campus Hungary fellowship programme. Funding for this project was partially provided by the Spanish Ministerio de Economa y Competitividad (MINECO) under projects FPA2012-39684, and Centro de Excelencia Severo Ochoa SEV-2012-0234. IS acknowledges support from NASA grants NNX12AF83G and NNX10AD53G.

REFERENCES

Abazajian K. N. et al., 2009, ApJS, 182, 543
Afshordi N., Slosar A., Wang Y., 2011, J. Cosmol. Astropart. Phys., 1101, 019
Biswas T., Notari A., 2008, J. Cosmol. Astropart. Phys., 0806, 021
Bremer M. N., Silk J., Davies L. J. M., Lehnert M. D., 2010, MNRAS, 404, L69
Cai Y. C., Neyrinck M. C., Szapudi I., Cole S., Frenk C. S., 2014, ApJ, 786, 110
Cardoso J.-F., Martin M., Delabrouille J., Betoule M., Patanchon G., 2008, IEEE J. Sel. Top. Signal Process., 2, 735
Colberg J. M., Sheth R. K., Diaferio A., Gao L., Yoshida N., 2005, MNRAS, 360, 216
Cruz M., Martinez-Gonzalez E., Vielva P., Cayon L., 2005, MNRAS, 356, 29
Cruz M., Tucci M., Martinez-Gonzalez E., Vielva P., 2006, MNRAS, 369, 57
Cruz M., Martinez-Gonzalez E., Vielva P., Diego J. M., Hobson M., Turok N., 2008, MNRAS, 390, 913
Das S., Spergel D. N., 2009, Phys. Rev. D, 79, 043007
DESI Collaboration:Levi M. et al., 2013, preprint (arXiv:1308.0847)
Driver S. P. et al., 2011, MNRAS, 413, 971
Euclid Collaboration:Laureijs R. et al., 2011, preprint (arXiv:1110.3193)
Euclid Collaboration:Amendola L. et al., 2013, Living Rev. Relativ., 16, 6
Francis C. L., Peacock J. A., 2010, MNRAS, 406, 14
García-Bellido J., Haugboelle T., 2008, J. Cosmol. Astropart. Phys., 0804, 003
Gorski K. M., Hivon E., Banday A. J., Wandelt B. D., Hansen F. K., Reinecke M., Bartelman M., 2005, ApJ, 622, 759
Granett B. R., Neyrinck M. C., Szapudi I., 2008, ApJ, 683, L99
Granett B. R., Neyrinck M. C., Szapudi I., 2009, ApJ, 701, 414
Granett B. R., Szapudi I., Neyrinck M. C., 2010, ApJ, 714, 825
Inoue K. T., 2012, MNRAS, 421, 2731
Inoue K. T., Silk J., 2006, ApJ, 648, 23
Inoue K. T., Silk J., 2007, ApJ, 664, 650
Inoue K. T., Sakai N., Tomita K., 2010, ApJ, 724, 12
Jarrett T. H., Chester T., Cutri R., Schneider S., Skrutskie M., Huchra J. P., 2000, ApJ, 119, 2498
Kaiser N., Burgett W., Chambers K., 2010, Proc. SPIE Conf. Ser.
Kofman L., Starobinsky A. A., 1985, SvA, 11, L271
Kovács A., Szapudi I., 2015, MNRAS, 448, 1305
Kovács A., Szapudi I., Granett B. R., Frei Z., 2013, MNRAS, 431, L28
Kovetz E. D., Kamionkowski M., 2013, Phys. Rev. Lett., 110, 171301
LSST Science Collaboration 2009, preprint (arXiv:e-prints)
Masina I., Notari A., 2009, J. Cosmol. Astropart. Phys., 0902, 019
Nadathur S., Lavinto M., Hotchkiss S., Räsänen S., 2014, Phys. Rev. D, 90, 103510
Papai P., Szapudi I., 2010, ApJ, 725, 2078
Planck Collaboration XII, 2013, preprint (arXiv:1509.06348)
Planck Collaboration XXIII, 2013, preprint (arXiv:1509.06555)
Planck Collaboration XIX, 2014, preprint (arXiv:1502.01594)
Rassat A., Starck J.-L., Dupé F.-X., 2013, A&A, 557, A32
Rees M. J., Sciama D. W., 1968, Nature, 217, 511
Romano A. E., Sanes S., Sasaki M., Starobinsky A. A., 2014, Europhys. Lett., 106, 69002
Rudnick L., Brown S., Williams L. R., 2007, ApJ, 671, 40
Sachs R. K., Wolfe A. M., 1967, ApJ, 147, 73
Schlegel D. J., Finkbeiner D. P., Davis M., 1998, ApJ, 500, 525
Skrutskie M. F. et al., 2006, AJ, 131, 1163
Smith K. M., Huterer D., 2010, MNRAS, 403, 2

Szapudi I., Prunet S., Pogosyan D., Szalay A. S., Bond J. R., 2001, ApJ, 548, L115
Szapudi I. et al., 2015, MNRAS, 450, 288
Tomita K., 2005, Phys. Rev. D, 71, 083504
Tomita K., Inoue K. T., 2008, Phys. Rev. D, 77, 103522
WMAP Collaboration:Bennett C. L. et al., 2013, ApJS, 208, 20
Wright E. L. et al., 2010, AJ, 140, 1868
Zhang R., Huterer D., 2010, Astropart. Phys., 33, 69
Zibin J. P., 2014, preprint (arXiv:1408.4442)

This paper has been typeset from a TEX/LATEX file prepared by the author.